Received: 6 September 2024 | Revised: 12 October 2024 | Accepted: 15 October 2024

DOI: 10.1002/dro2.153

RESEARCH ARTICLE

Droplet WILEY

Programmable optical window bonding enabled 3D printing of high-resolution transparent microfluidic devices for biomedical applications

Mengguang Ye[1] | Yuxiang Xue[1] | Hongyu Zhao[2] | Patricia Hazelton[1] | Yuxuan Ji[1] | Glen McHale[2] | Xianfeng Chen[1]

[1]Institute for Bioengineering, School of Engineering, The University of Edinburgh, Edinburgh, UK

[2]Institute for Multiscale Thermofluids, School of Engineering, The University of Edinburgh, Edinburgh, UK

Correspondence
Xianfeng Chen, Institute for Bioengineering, School of Engineering, The University of Edinburgh, Edinburgh EH9 3JL, UK.
Email: Michael.Chen@ed.ac.uk

Abstract

Traditional technologies for manufacturing microfluidic devices often involve the use of molds for polydimethylsiloxane (PDMS) casting generated from photolithography techniques, which are time-consuming, costly, and difficult to use in generating multilayered structure. As an alternative, 3D printing allows rapid and cost-effective prototyping and customization of complex microfluidic structures. However, 3D-printed devices are typically opaque and are challenging to create small channels. Herein, we introduce a novel "programmable optical window bonding" 3D printing method that incorporates the bonding of an optical window during the printing process, facilitating the fabrication of transparent microfluidic devices with high printing fidelity. Our approach allows direct and rapid manufacturing of complex microfluidic structure without the use of molds for PDMS casting. We successfully demonstrated the applications of this method by fabricating a variety of microfluidic devices, including perfusable chips for cell culture, droplet generators for spheroid formation, and high-resolution droplet microfluidic devices involving different channel width and height for rapid antibiotic susceptibility testing. Overall, our 3D printing method demonstrates a rapid and cost-effective approach for manufacturing microfluidic devices, particularly in the biomedical field, where rapid prototyping and high-quality optical analysis are crucial.

INTRODUCTION

Microfluidic devices are becoming increasingly vital in biomedical research because of their ability to manipulate small volumes of fluids for a variety of applications, such as drug delivery and lab-on-a-chip systems.[1] Polydimethylsiloxane (PDMS) is a commonly used elastic material for fabricating microfluidic devices because of its low cost, high transparency, biocompatibility, and ease of fabrication.[2] However, traditional PDMS-based microfluidic devices fabricated through soft lithography have several limitations. The fabrication process is complex, requiring specialized equipment and expertise, which makes it costly and time-consuming to iterate and optimize designs. Additionally, PDMS-based devices are limited in the aspect ratio of their structures due to the material's tendency to deform.[3]

To overcome these issues, researchers have explored 3D printing as an alternative method for fabricating microfluidic devices.

Three-dimensional (3D) printing enables rapid prototyping and customization of complex microfluidic structures and has the potential to significantly reduce the cost and time required for microfluidic device fabrication, as well as the need for designated facilities. Digital light processing (DLP) is a 3D printing technology that uses ultraviolet (UV) light to polymerize photosensitive resins layer by layer, typically utilizing a digital micromirror device (DMD) to project images of each layer onto the resin, causing it to cure and solidify.[4] DLP-3D printing is known for its high resolution and fast printing speeds, making it a preferred choice for producing microfluidic devices. Despite their advantages, 3D-printed microfluidic devices face inherent challenges, such as opacity, low surface quality, high cytotoxicity, and limitations in printing resolution and fidelity. These issues can significantly restrict their practical application in the field of microfluidics.[5,6] There are three main approaches to creating microfluidic devices using the DLP-3D printing technology: direct printing, mold-based (indirect), and hybrid approach.[7]

In the direct printing method, a monolithic microfluidic device is printed directly, whereas the indirect method involves printing a template for PDMS casting, which is then used to produce the final product. The mold-based approach is similar to soft photolithography, but it is generally more affordable and accessible. However, PDMS will not cure properly on 3D-printed molds made from most commercially available photopolymer resins due to the release of a variety of chemicals from 3D-printed molds, including polyethylene glycols, diethyl-phthalates,[8] unreacted monomers,[9] and phosphineoxide photoinitiators.[10] These substances inhibit the Pt-based catalyst for the curing process of PDMS.[11] As a result, additional processing steps, such as temperature control, coating, silanization, etc., are usually required to facilitate PDMS curing on the surface of 3D-printed molds.[12–14] In contrast, the direct method tends to be more efficient and time saving, allowing greater control to produce intricate designs. Nevertheless, monolithic microfluidic devices fabricated through direct printing are commonly opaque and incompatible with microscopes, despite employing clear resin and post-printing polishing to enhance the device's transparency. The reason is that the surfaces of 3D-printed microfluidic devices are often rough and irregular, causing light scattering and making it difficult to obtain clear images when studying the research phenomena happening within the inside of the 3D-printed microfluidic devices.[15,16] Direct printing on glass can mitigate some issues, but the suction force during printing can distort the roof layer, compromising the quality of subsequent layers.

To address these transparency issues, a hybrid approach has been developed that uses adhesive materials (such as double-sided adhesive tape or UV glue) to bond the printed device to a transparent plate. However, each of these methods introduces new challenges. For example, manually positioning adhesive tape to align with the microfluidic device's pattern is difficult due to the small size and complexity of the pattern. Using UV glue requires careful application to ensure even distribution and avoid obstructing microchannels, which limits this method to devices with coarse features and well-separated channels. Additionally, despite advancements in 3D printer achieving resolution down to 10 μm in-plane, creating channels narrower than 100 μm in the layer building direction remains challenging due to material limitations.[17] This occurs because UV light transmitted through previously built layers can over-cure the resin within channels, leading to rough surfaces or blockages that negatively impact device performance and functionality.[18,19]

To further improve 3D printing technologies for fabrication of microfluidic devices, herein, we present a novel "programmable optical window bonding" 3D printing (POWB-3DP) method that involves first printing the microfluidic device directly onto a glass substrate, followed by bonding the device with a coverslip. This POWB-3DP method overcomes current limitations of 3D-printed microfluidic devices, enabling the rapid and direct manufacturing of complex microfluidic structures with high accuracy and smooth surface quality. By integrating these steps into a streamlined manufacturing process, our POWB-3DP method offers a cost-effective (material cost <£1), time-efficient (<1 h), and convenient solution for the production of microfluidic devices, making it particularly suitable for experiments requiring iterative design. To demonstrate its effectiveness, we fabricated a range of microfluidic devices and evaluated their performance, positioning our technology an attractive option for researchers and engineers seeking to rapidly prototype and evaluate new microfluidic designs. Overall, our POWB-3DP method offers a rapid, cost-effective, and versatile solution for the 3D printing of high resolution, complex microfluidic devices, making it an invaluable tool for advancing the design and development of microfluidic systems across various biomedical applications.

RESULTS AND DISCUSSION

To address the challenges of opacity, resin over-curing by transmitted UV light, low surface quality, and low printing resolution in 3D-printed microfluidic devices, we developed a novel POWB-3DP method that incorporates a transparent optical window during printing and employs a precise bonding technique. This approach resulted in transparent microfluidic devices compatible with optical assessments and enabled accurate manufacturing without compromising device features.

For this process, we selected the Asiga MAX X printer, an advanced desktop 3D printer utilizing DLP technology. The Asiga MAX is equipped with a 1080P projector and 385 nm UV light, offering a 27 μm pixel resolution on the XY plane. The 385 nm wavelength was selected over the 405 nm wavelength due to its superior efficiency in printing transparent resins.[16] Furthermore, a DLP printer was chosen over an MSLA printer because DLP technology offers higher light uniformity and eliminates issues with UV light bleed-through, ensuring precise curing of the bonding layer. Our innovative POWB-3DP technique can be broken down into the following key steps, each carefully designed to ensure the fabrication of high quality and functionality of the microfluidic device (Figure 1a):

1. *Printing the base plate*: This step begins by printing a plate that serves as a platform for the next steps. This plate provides a smooth surface and ensures proper alignment for attaching a glass coverslip.

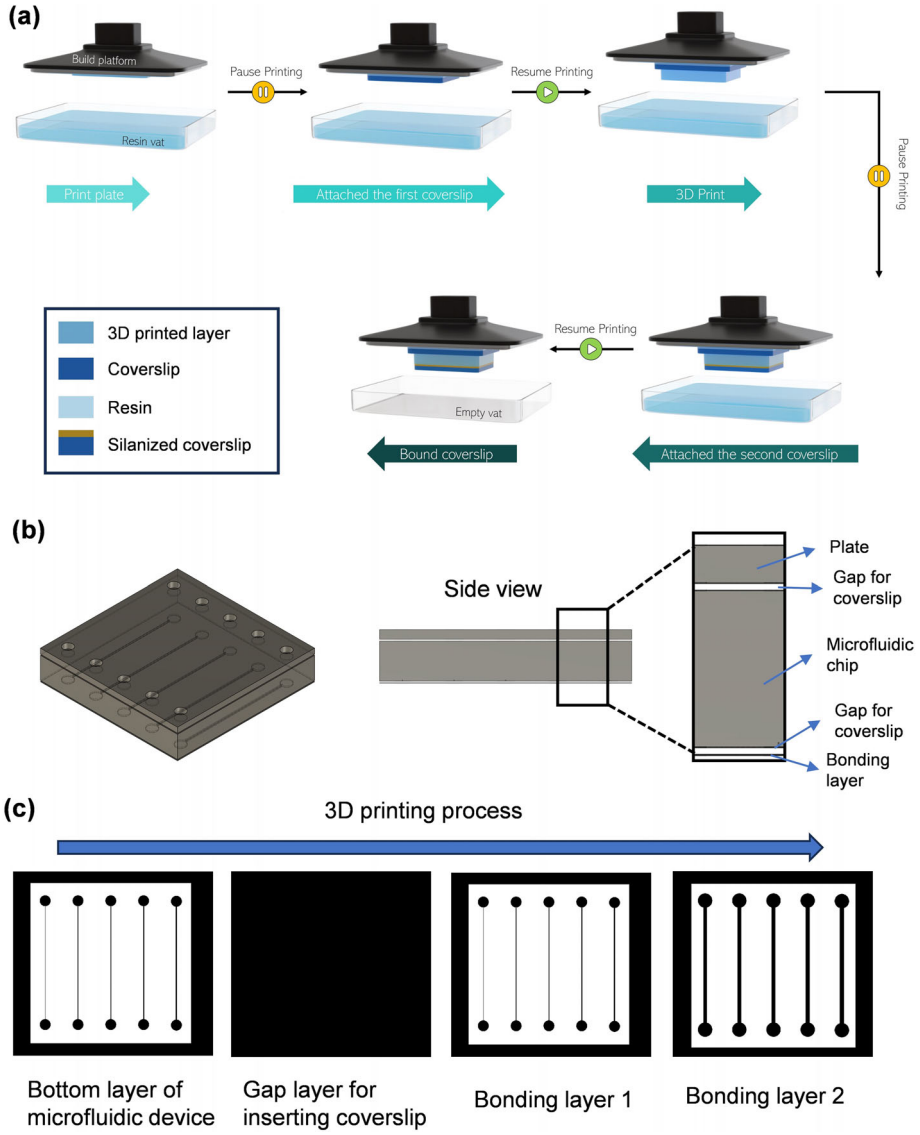

FIGURE 1 Principle of the "programmable optical window bonding" 3D printing (POWB-3DP) method for fabricating microfluidic devices. (a) Schematic of the manufacturing process: This panel illustrates the steps involved in creating a microfluidic device using 3D printing. Initially, the 3D printer builds a base plate designed to hold a coverslip, which will later be used to fabricate the microfluidic device. After the completion of the microfluidic structure, the printing process is paused to allow for the attachment of a silanized coverslip, preparing it for the bonding procedure that follows. (b) Three-dimensional model design for microfluidic devices: this panel shows the specific design features of the 3D model used for printing microfluidic devices. It highlights the innovative aspects of the 3D printing approach, emphasizing how the design is tailored to accommodate the subsequent bonding steps. (c) Bonding principle: a gap layer is included to accommodate the insertion of the silanized coverslip. Bonding layer 1 mirrors the bottom layer of the microfluidic device, ensuring a seamless connection with the fabricated structure. Bonding layer 2 features expanded borders around the microchannels to enhance the overall bonding strength. Bonding layers 1 and 2 are printed using an empty vat. The purpose is to make use of programmed 3D printer ultraviolet (UV) illumination to localize bonding to required locations. The white pattern represents the UV-illuminated image projected onto the coverslip (the bottom of the printed microfluidic device), which specifically polymerizes the resin in the exposed (white) areas, resulting in bonding to coverslip.

2. *Attaching the coverslip*: The printing process is paused to attach a coverslip onto the printed plate. Once the coverslip is securely in place, the printing is resumed, allowing the microfluidic device to be printed directly onto the attached coverslip.
3. *Finalizing the microfluidic device*: After completing the final layer of the microfluidic device, the print is paused again to remove any excess resin from the bottom of the device.
4. *Bonding the silanized coverslip*: Another silanized coverslip is placed on top of the microfluidic chip. Silanization is to form bonding between the coverslip and the microfluidic chip under UV illumination. The resin vat is replaced with an empty one, and the build platform is repositioned to print two additional layers. These layers are not printed on the glass surface but instead serve to bond the silanized coverslip to the bottom of the microfluidic device at specific, predetermined areas.

5. *Post-processing*: The final step involves removing the printed microfluidic device from the build platform and detaching the plain coverslip with ease. The device then undergoes a washing process to remove any residual resin from the microfluidic channels, ensuring its functionality and cleanliness.

The design of the 3D printing model for the microfluidic chips includes three main components: the base plate for attaching the coverslip, the microfluidic chip itself, and a thin bonding layer for securing the silanized coverslip (Figure 1b). The 3D printing model incorporates two gaps designed to accommodate the coverslip during printing, with thicknesses matched to the coverslip used. The printing process is paused after the final layer of the gap is completed to allow for the attachment of the coverslip before continuing with the subsequent steps. The dimensions of the coverslip do not need to match the exact size of the microfluidic device, as long as it effectively seals the microchannels. The coverslip can be smaller or larger without compromising functionality, as long as it covers the critical channel areas. However, the thickness of the designed gap should correspond to the thickness of the coverslip to prevent mechanical interference during printing, which could damage the printer or disrupt the structural integrity of the printed device. Regarding fluid entry points, it is important to note that the coverslip itself does not require pre-cut holes. Fluid entry is accommodated by the 3D-printed structure, which includes built-in inlet and outlet ports. The coverslip's role is to seal the channels and provide an optical window to the printed microfluidic devices.

The precise bonding mechanism between the coverslip and the microfluidic device is achieved through the use of programmed 3D printer UV illumination. This method ensures that the bonding is not only strong but also at precise location, avoiding common issues such as distortion or channel blockage as UV light illumination cannot be precisely localized to the locations where bonding between microfluidic device and coverslip is required. The bonding is achieved via printing two layers from empty vat (Figure 1c). The first layer is patterned to match the bottom layer of the microfluidic device, ensuring a seamless bond. The exposure time for this layer is critical: if too short, the bond may be weak and prone to distortion during the washing process; if too long, it might cause blockage or distortion of the channels. The second layer features an expanded border to enhance bonding strength without affecting the channels. This elegant design allows for a longer exposure time, preventing delamination and ensuring that the silanized coverslip remains securely attached while preserving the designed channel.

With this mechanism, we fabricated an array of microfluidic devices using both our POWB-3DP technique and compared them to those made using glue bonding approach reported in the literature. We first implemented our POWB-3DP method via an entry-level DLP-3D printer (Anycubic). Despite this printer offering only 80 μm pixel resolution on the XY plane, its affordability (less than £500) makes it widely accessible. As shown in Figure 2, all devices created with our method produced high-quality channels, as indicated by the clear flow of blue fluid. In contrast, devices bonded with UV glue encountered issues such as either incomplete bonding, indicated by an intermittent flow pattern within the channel, or channel blockage, evident from the partially filled flow at the liquid injection point. These problems arise because manually applying UV glue to bond the microfluidic chip to the glass is challenging. The precision needed is difficult to achieve manually. Excess glue can easily obstruct the channels, while insufficient UV glue can lead to incomplete bonding, resulting in fluid leakage and other issues.

It is crucial for 3D-printed microfluidic devices to meet both fundamental and specialized requirements, such as high optical transparency and printing fidelity. In the previous section, we introduced our innovative POWB-3DP method for rapidly prototyping microfluidic devices by bonding a glass window during the printing process. While many other 3D printing techniques have been developed to achieve transparent microfluidic devices with high fidelity, in this section, we compare these methods and highlight the advantages of our technology.

First, we fabricated a microfluidic chip and compared it with those produced using other current 3D printing techniques, including conventional direct 3D printing, UV glue bonding, and printing on silanized glass. The chip feature spiral and serpentine (parallel channel section) channels with a constant channel height of 100 μm. The spiral channel has a width of 500 μm, while the serpentine channel is 200 μm wide. The widths of inlets are 420 and 80 μm (Figure 3a,b, labeled "POWB-3DP").

The results demonstrated that the microfluidic devices created with our method were successfully fabricated, as indicated by the clear flow through the entire channel (Figure 3b,c, labeled "POWB-3DP"), and the high-quality channel structures (Figure 3b,c, labeled "POWB-3DP"). In contrast, chips produced from conventional direct 3D printing approach were opaque, with all channels blocked (Figure 3c, labeled "original direct print"). This blockage occurs because UV light transmitted through previous layers causes resin over-curing, leading to channel obstructions. While printing on silanized glass improved device transparency, it did not resolve the over-curing issue (Figure 3b,c, labeled "print on glass").

We again compared the conventional hybrid approach of 3D printing followed by UV glue bonding. This method resulted in blocked channels, where fluid cannot flow due to blockage caused by the bonding technique (Figure 3b,c, labeled "UV glue"). Additionally, glue residual was visible in the microchannels (Figure 3b,c, labeled "UV glue").

When printed the device shown in Figure 3a, which features a constant channel height of 100 μm, the channel of the device printed on silanized glass was completely blocked (Figure 3b,c). Therefore, it is not possible to directly compare the transparency of the channel between the devices printed by our method (labeled "POWB-3DP") and the method printed on glass (labeled "print on glass") or by conventional 3D printing method (labeled "original direct method"). To enable direct comparison between the methods, the channel should be designed with sufficient height to prevent blockage from transmitted UV light when building the roof layer. For this, we made a new device, as illustrated in Supporting Information: Figure S1a with a channel height of 800 μm by these three methods and then evaluated the optical transparency of these devices. The device printed on glass is presented in Supporting Information: Figure S1b. It can be seen that

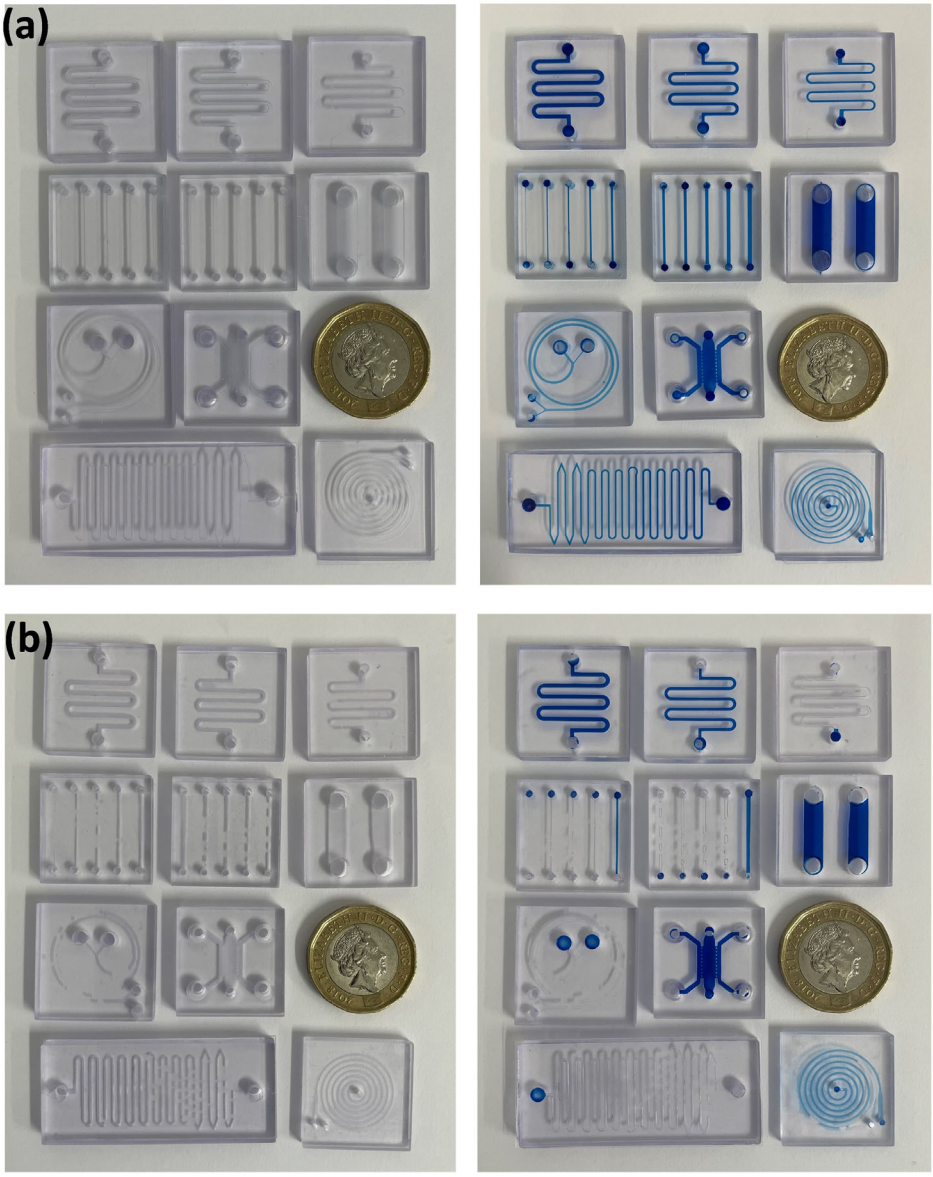

FIGURE 2 Comparison of 3D-printed microfluidic chips using our "programmable optical window bonding" 3D printing (POWB-3DP) technique and the glue bonding method reported in the literature. (a) Microfluidic chip produced with our POWB-3DP method. (b) Microfluidic chip fabricated using traditional glue bonding method. A blue fluid was added to indicate the flow in microchannels.

the surface quality of the channel is poor, as indicated by the white bubbles within the channel. The device fabricated using conventional hybrid approach of using UV glue was excluded from the optical assessment as this method resulted in blocked channels, making it unsuitable for microfluidic device fabrication. To test the transparency of the microfluidic devices fabricated by the three methods, we introduced fluorescent microbeads of two different sizes (7 μm [green] and 20 μm [red]) into the channels followed by fluorescence microscopy observation. It can be seen that our method resulted in channels with high optical transparency and smooth surface finishes on both the roof (Figure 3d, labeled "top") and floor layers (Figure 3d, labeled "bottom"). While devices printed on silanized glass also demonstrated good optical transparency, they suffered from poor surface quality on the roof layer (Figure 3d, labeled "top" and Supporting Information: Figure S1b). This is a common issue in 3D-printed microfluidics, arising due to suction forces between the printed layers and the transparent film of the resin vat during the printing process, which distorted the roof layer of channel. The microfluidic devices printed from conventional 3D printing technique (named "original direct print" in Figure 3b) showed poor optical transparency and encountered similar surface quality issues as those printed on glass (Figure 3b,e, and Supporting Information: Figures S1, S2). Only red fluorescence (20 μm microbeads) was able to be observed from the device fabricated using the original direct print method. Green fluorescent beads could not be imaged with a clear focus due to the channel's very poor transparency (Figure 3e).

Adjusting the printing orientation may improve the printability of microfluidic devices. However, this adjustment can increase surface roughness due to the layer-by-layer deposition inherent in

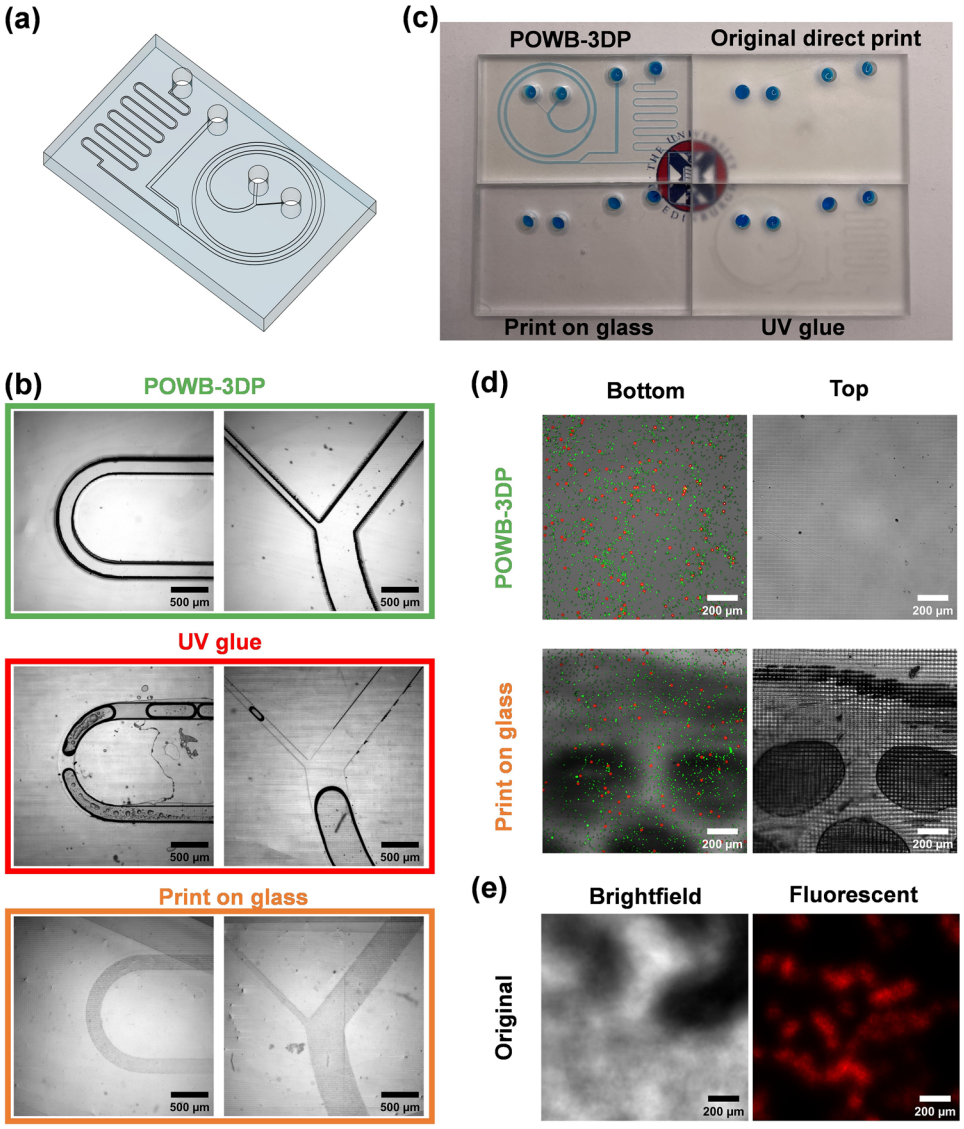

FIGURE 3 Comparison of 3D-printed microfluidic chips. (a) Three-dimensional (3D) model of the microfluidic chip. (b) Comparison of 3D-printed microfluidic chips produced using different methods, labeled "programmable optical window bonding" 3D printing ("POWB-3DP"), "original direct print" (conventional 3D printing method), "print on glass" (modified 3D printing on glass to improve transparency), and "UV glue" (3D printing followed by conventional UV glue bonding as reported in the literature). (c) Bright-field images of 3D-printed channels produced by POWB-3DP method, UV glue, original direct printing and direct printing on silanized glass. (d) Channels printed on silanized glass displayed poor surface quality on the roof layer (labeled "top"). In contrast, channels produced using our method exhibited superior surface quality and high optical transparency. Green and red colors indicate 7- and 20-μm microbeads, respectively. (e) The microfluidic device fabricated by conventional 3D printing method (labeled "original") showed poor optical transparency.

DLP-3D printing, resulting in an opaque appearance that impacts the optical properties of the printed object (Supporting Information: Figure S4a). Additionally, altering the orientation only improves the printability of microchannels aligned parallel to the printing direction.

Additionally, researchers have also attempted to fabricate microfluidic devices from 3D-printed mold. Supporting Information: Figure S3 highlights the challenges associated with this technique, which often result in incomplete PDMS curing. These findings underscore the effectiveness of our POWB-3DP method in achieving precise and durable bonds (Figures 2a, 3, and Supporting Information: Figure S4b,c).

We admitted that with careful modifications of these techniques, such as surface treatments of 3D-printed molds for subsequent PDMS casting,[20,21] utilizing specially formulated resins to enhance transparency and fidelity,[16,22] and employing customized 3D printers with ultra-high resolution capabilities,[23] it is possible to fabricate relatively high-quality microfluidic devices. However, these methods often require complex procedures, precise calibration, specialized materials, and advanced equipment, which can significantly increase both the time and cost of fabrication. While achieving high printing resolution with customized 3D printers equipped with advanced hardware is feasible, producing channels with smaller dimensions in the *Z*-direction

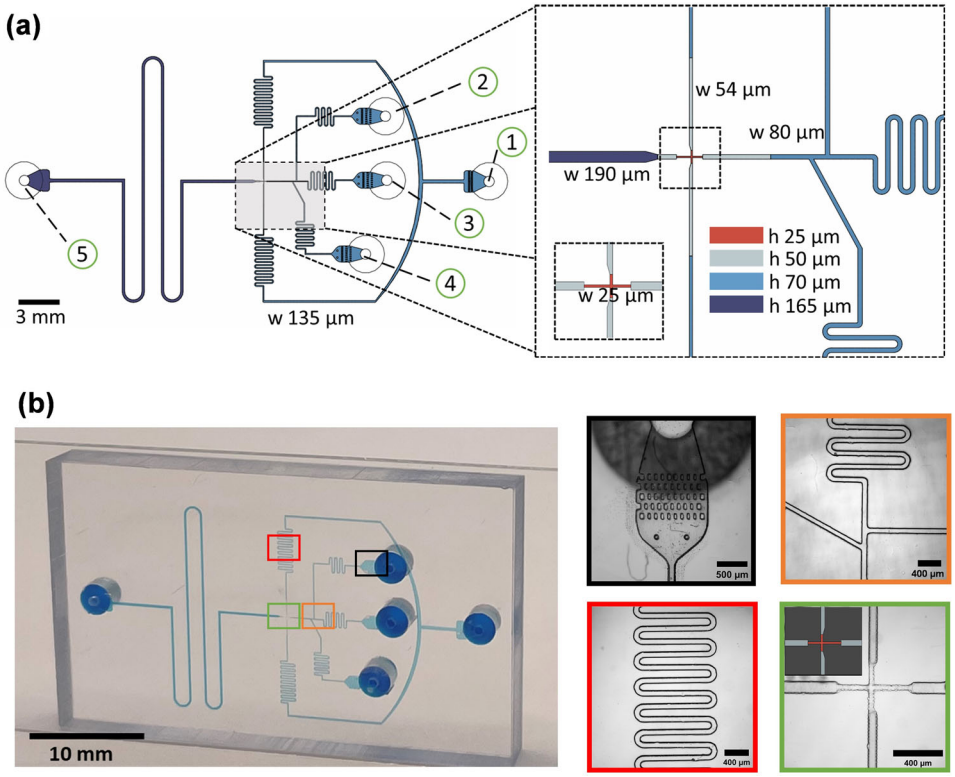

FIGURE 4 Characterization of the 3D-printed droplet microfluidic device. (a) Design of droplet microfluidic device for single-cell encapsulation of bacteria. (1) Input channel for the fluorinated oil with mixing surfactant. (2 and 4) Input channel for loading antibiotic. (3) Input channel for the bacteria sample containing cell viability indicator. (5) Output channel for collection of droplets. (b) Photograph of 3D-printed droplet microfluidic device. Optical images showcase the 3D-printed droplet microfluidic device. Key design features are presented including passive filter (black), flow resistors (orange and red), and a flow-focusing nozzle (green) (scale bar: 200 µm).

(layer-building direction) remains challenging due to the inherent issue of resin over-curing.[17] Overall, we believe that our technique offers the advantage of producing microfluidic devices with higher transparency and fidelity through simpler and more reproducible procedures.

As one example to demonstrate the application of our 3D-printed microfluidic devices, we create a droplet microfluidic device featuring optical transparency, high printing fidelity, cost-effectiveness, and time efficiency. The device features a design with four height regions and a flow-focusing nozzle that measures 25 µm in both height and width. The four height regions are indicated by four different colors. The red color represents the flow-focusing nozzle with a microchannel height of 25 µm. The upstream microchannels, which converge at the flow-focusing nozzle with a length of approximately 1.5 mm, and a short section of 0.25 mm downstream of the nozzle, are colored light blue, indicating a height of 50 µm (Figure 4a). The remaining upstream and downstream microchannels, with heights of 70 and 165 µm, are represented in blue and dark blue, respectively (Figure 4a). To reduce flow resistance, the width of the downstream serpentine microchannel expands from 25 µm at the flow-focusing nozzle to 190 µm, making it the tallest and widest channel in the microfluidic platform. The dimensions of the upstream microchannels are 80 µm wide for the aqueous phase (Figure 4a, the inlets labeled "2," "3," and "4") and 54 µm wide for the oil phase (Figure 4a, the inlets labeled "1"), culminating at the flow-focusing nozzle region where the dimensions are 25-µm tall and 25-µm wide (Figure 4b, microscope image within the green box). The heights of microchannels are strategically optimized to facilitate the high-throughput production of droplets. In order to prevent clogging of the flow-focusing nozzle, passive filters (the blue regions next to the inlets labeled "1," "2," "3," and "4") were designed and incorporated at inlets (Figure 4b, microscope image within the black box). Additionally, flow resistors (serpentine channels) were designed for both oil and aqueous phases to dampen fluctuations arising from the mechanical instability of syringe pumps (Figure 4b, microscope image within the red and orange boxes). Attractively, our microfluidic device is fully transparent, which enables in situ droplet observation by optical microscopy in the future. The height of the microchannels were confirmed using DektakXT (Supporting Information: Figure S5).

In this study, we employed the 3D-printed droplet microfluidic device to generate droplets. Before conducting the experiment, we coated the microfluidic device channel surfaces with a hydrophobic surface coating agent, thereby enhancing the performance and stability of aqueous droplets in fluorinated oils during the droplet generating process. This procedure was crucial to generate monodispersed droplets with precise volume and reproducible antibiotic susceptibility testing (AST) results in the end. Notably, the 3D-printed droplet microfluidic device has demonstrated excellent performance for at least several months, which is the duration of the current test period. Two types of oil (Fluo-Oil 200 and Fluo-Oil 7500) were

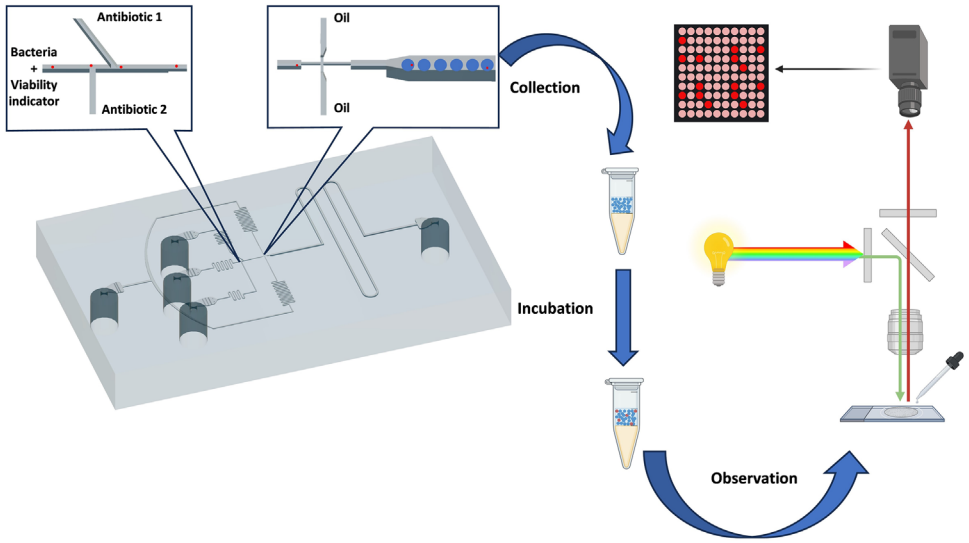

FIGURE 5 Overview of the 3D-printed droplet microfluidic platform for rapid antibiotic susceptibility testing (AST). This platform facilitates the encapsulation of bacterial cell, along with a fluorescent bacterial growth indicator dye and antibiotics, into picolitre-sized droplets. These droplets are then collected and incubated at 37°C in darkness prior to assessment under a fluorescent microscope. In the microfluidic device, the red dots represent bacteria, and the blue spheres represent aqueous droplets. After incubation, the red spheres in the Eppendorf tube represent droplets containing bacteria that emit fluorescence signals.

evaluated for their effectiveness in droplet generation. Regarding droplet size, droplets produced with Fluo-Oil 200 were generally smaller than those made with Fluo-Oil 7500 at the same aqueous-to-oil phase flow ratio, which was attributable to the higher viscosity of Fluo-Oil 200 (Supporting Information: Figure S6).

Next, we optimized the design of the flow-focusing nozzle to generate stable, monodisperse droplets with the desired volume. We aimed to minimize the volume of the generated droplets by optimizing both the flow-focusing nozzle and the flow rate ratio between the oil and aqueous phases. We chose to use AlamarBlue reagent, a reagent that can be converted from weakly fluorescent resazurin to strongly fluorescent resorufin under the cellular reducing environment, as a cell viability indicator for AST. Droplets with smaller volumes are more sensitive to changes in resorufin concentration. The dimensions of the flow-focusing nozzle play a critical role in determining both the size and uniformity of the generated droplets. Initially, a flow-focusing nozzle with dimensions of 54 μm produced droplets with a diameter of 145 μm, which were too large for rapid AST (Supporting Information: Figure S7). By refining the nozzle dimensions to 25 μm, we achieved smaller, monodisperse droplets with a diameter of 43 μm (40 pL). Further reduction in droplet size to 33 μm (18 pL) was accomplished by adjusting the flow ratio of the aqueous to oil phase (Supporting Information: Figure S8). Supporting Information: Table S1 summarizes the sizes of droplets generated under various conditions, including the size of flow-focusing nozzles, the flow rate ratio of the aqueous to oil phase, and the type of carrier oil.

Before conducting bacterial encapsulation and AST, we optimized the generation of 18 pL monodispersed droplets using the 3D-printed microfluidic device, which enhanced the detection sensitivity of bacterial growth. We discovered that selecting the right fluorinated carrier oil is crucial for fluorescence detection. Fluo-Oil 7500 showed low dye retention, leading to indistinguishable fluorescence signals between droplets with and without bacteria (Supporting Information: Figure S9). To address this, we switched to Fluo-Oil 200, which significantly improved dye retention and allowed clear differentiation between empty droplets and those containing bacteria after 3 h of incubation (Supporting Information: Figure S10).

Each droplet contained the cell viability indicator, AlamarBlue, along with antibiotics. Upon entering bacteria, this weakly fluorescent compound is reduced to resorufin which is a strongly fluorescent molecule with a red color. Due to the ultra-small volume of the droplets, the fluorescence signal is significantly amplified, allowing us to clearly differentiate droplets encapsulating actively growing bacteria from those that encapsulate no bacteria or where bacterial growth is inhibited by the antibiotics.

The design of using our microfluidic devices for AST is illustrated in Figure 5. Initially, antibiotics are introduced into the inlets for the aqueous phase. Droplets are formed at the flow-focusing nozzle, where the aqueous and immiscible oil phases meet. Following collection of the droplets from the outlet into Eppendorf-type tubes, the sample was incubated at 37°C in the dark prior to subsequent analysis. Following incubation, 10 μL of emulsion was carefully pipetted onto a microscope slide for microscopy observation. Finally, fluorescence signals from all droplets were recorded and analyzed to assess and quantify bacterial growth post-incubation.

Based on this design, we performed AST using droplets to see if rapid AST can be achieved. We introduced *Escherichia coli* spiked in Muller Hinton (MH) broth along with AlamarBlue reagent, accompanied by either ampicillin (8 μg/mL) or ciprofloxacin (1 μg/mL). These concentrations were selected based on the U.S. Clinical and Laboratory Standards Institute-recommended interpretive breakpoint concentrations for Enterobacterales to categorize the bacteria as either

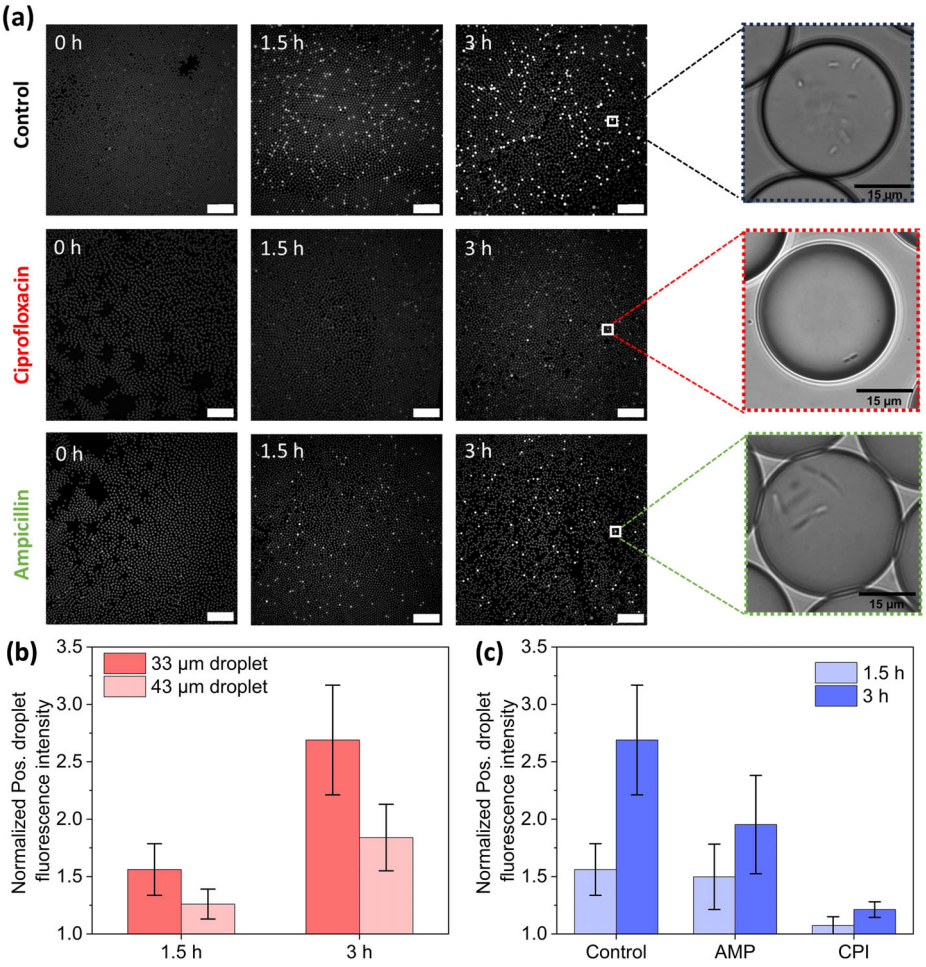

FIGURE 6 Quantitative analysis of bacterial growth for antibiotic susceptibility testing (AST). (a) Fluorescence images showing bacterial growth in droplets after 1.5 and 3 h of incubation without antibiotics (control group), with 1 μg/mL ciprofloxacin (CIP), or with 8 μg/mL ampicillin (AMP), and bright-field micrographs illustrating bacterial growth after 3 h of incubation (scale bar: 400 μm). (b) Quantitative analysis of normalized fluorescence intensity in droplets of 33 and 43 μm diameters after 1.5 and 3 h of incubation. (c) Quantitative analysis of normalized fluorescence intensity at 1.5 and 3 h following treatment with CIP and AMP compared with no antibiotic addition.

susceptible (S) or resistant (R). The *E. coli* strain DB3.1 was selected for its resistance to ampicillin and susceptibility to ciprofloxacin (Supporting Information: Figure S11). The positive droplets represent those containing bacteria, which exhibit high fluorescent intensity, suggesting high bacterial concentration (control and ampicillin groups in Figure 6a). In contrast, the negative droplets represent those without bacteria, characterized by emitting a weak fluorescent signal and visual verification by bright-field images (ciprofloxacin group) as bacterial growth was effectively inhibited. Fluorescence intensities were quantitatively measured for both positive and negative droplets. The data were then normalized by comparing the fluorescence intensities of the positive droplets to the average intensity of the negative droplets (background fluorescent signal). In the control group, the normalized fluorescence intensity of positive droplets was 1.56 ± 0.22 at 1.5 h and 2.69 ± 0.48 at 3 h. When treating *E. coli* with ampicillin, there was no noticeable change in fluorescence intensity compared with that of the control group at 1.5 h (1.50 ± 0.28 in ampicillin-treated group vs. 1.56 ± 0.22 in the control group), whereas the bacteria proliferation rate was slightly reduced at 3 h (1.95 ± 0.43 vs. in the ampicillin-treated group vs. 2.69 ± 0.48 in the control group) (Figure 6a,c). In contrast, after administering ciprofloxacin, the inhibition of bacterial growth was noted at 1.5 h, as demonstrated by the low normalized fluorescence intensity: 1.07 ± 0.08 at 1.5 h and 1.21 ± 0.07 at 3 h (Figure 6a,c). Therefore, the preliminary results clearly demonstrate that we are able to conclude ciprofloxacin is effective in bacteria inhibition while ampicillin is ineffective, within only 1.5 h. This rapid detection arises from our ability to produce uniform, stable, and ultra-small droplets. The smaller-volume droplet (18 pL) was preferred for conducting rapid AST because it provides a more amplified signal with higher contrast over the same period compared to a larger-volume droplet (40 pL) (Figure 6b). In the future, antibiotics at varying concentrations can be introduced to the device using a computer-controlled pump, allowing for the determination of the minimum inhibitory concentration of antibiotics.

In addition to 3D-printed microfluidic devices for rapid AST, we further demonstrated the utility of our microfluidic devices in biomedical applications, such as enabling clear imaging of biological systems within the microchannels and facilitating spheroid formation due to their high

biocompatibility and transparency (Supporting Information: Figures S12–S15). In summary, our approach effectively overcomes the current challenges associated with 3D-printed microfluidic devices, producing high-quality and transparent microfluidic chips with straightforward printing procedures.

CONCLUSION

In this work, we introduced a straightforward and cost-efficient POWB-3DP method for rapidly prototyping microfluidic devices, effectively eliminating the need for traditional photolithography, which requires cleanroom access and specialized training. Our innovative POWB-3DP technique addresses the inherent limitations typically associated with 3D printing in microfluidic device fabrication, such as opacity, over-curing of the resin by transmitted UV light, low surface quality, and low printing fidelity. Additionally, our POWB-3DP method allows for the rapid manufacturing of microfluidic devices with features tailored to specific experimental needs, all without significant time and cost investments. This advancement is particularly beneficial for laboratories that require iterative design and testing.

We validated our approach using two different types of 3D printers: an entry-level Anycubic 3D printer (costing less than £500) and a more advanced, higher-resolution Asiga 3D printer. This demonstrates the versatility and universality of our POWB-3DP method, showing that it can be successfully implemented across a range of 3D printers, from basic to sophisticated models. This flexibility ensures that even small research groups or companies with limited resources can adopt our approach to design and fabricate microfluidic devices for various applications, without compromising on quality or transparency. Our results confirmed that microfluidic channels could be fabricated with fine resolutions, adapting well to the capabilities of different 3D printers without causing blockages or loss of fidelity. We believe that our approach is more straightforward and easier to replicate than existing methods, as demonstrated by the ability to manufacture microfluidic channel features as small as one pixel size of the 3D printer's resolution, without blockages or fidelity loss. In conclusion, our facile POWB-3DP method shows significant potential as an alternative method for manufacturing microfluidic devices, particularly in biomedical research.

METHODS

PlasClear V2 resin was purchased from Apply3D. Formlabs BioMed Clear resin was purchased from Solid Print3D. Bovine serum albumin, phosphate-buffered saline solution, isopropanol, LB broth, and LB agar were purchased from Sigma–Aldrich. Anti-adherence rinse solution was purchased from STEMCELL Technologies. Cleaning Fluid Bio was purchased from 3Dresyns. Fluo-oil 200, FluoSurf Surfactant, Fluo-Oil 7500, and hydrophobic surface treatment solution were purchased from Darwin Microfluidics. AlamarBlue was purchased from Thermo Fisher Scientific.

All printed objects used for this work were designed in Autodesk Fusion 360 2022 and exported as a .STL file. Files were then opened in the slicer software of Photon Workshop or Asiga Composer, where prints would be converted into a correctly sliced file for printing with an appropriate layer height. The corrected sliced file was transferred to the 3D printers. The principle behind DLP printing involves using a digital light projector to selectively cure liquid photopolymer resin into solid objects through a process called vat photopolymerization.

After printing, all devices were first rinsed with fresh isopropanol and sonicated for 1 min to wash off the excess resin residue on the surfaces. After washing, a vacuum pump was used to remove excess resin trapped in the channels. Then, the Cleaning Fluid Bio (3Dresyns, P11189) was used to rinse the channels and the devices were sonicated for an additional 10 min. After washing, devices were soaked in fresh isopropanol for 2 min to remove the cleaning fluid and dried with compressed air or placed in a dry and dark place for at least 30 min to ensure that the prints were completely dried before post-curing using the Form Cure station (Formlabs). In order to achieve the optimized the mechanical properties and biocompatibility of printed devices (Formlabs BioMed Clear resin), the curing time and temperature were set at 60 min and 60°C, as indicated by the manufacturer's guideline. In terms of the printed microfluidic devices using Asiga PlasClear resin, the curing time was 15 min at room temperature.

The coverslips were thoroughly cleaned with acetone, isopropyl alcohol, and deionized (DI) water and then dried using pressurized air and surface was activated in an oxygen plasma oven. To silanize the coverslips, 0.8 mL of TMSPMA was sprayed onto a piece of paper and placed in a vacuum desiccator overnight. Silanization was achieved by the evaporation of TMSPMA onto the coverslips. The silanized coverslips were stored in the desiccator until use.

Three-dimensional-printed microfluidic devices were placed under an inverted fluorescence microscope (DMi8 Leica) for characterization. Bright-field or fluorescent images were taken for the subsequent measurement of channel widths for assessment printing accuracy on the *XY* plane or *Z*-axis, respectively. The deviation between the designed values and actual measurements was determined by comparing the designed and measured values. Any deviations between the two sets of values were analyzed and evaluated to assess the level of accuracy of the printed devices.

Prior to experimentation, the 3D-printed droplet microfluidic device underwent a thorough flush with a hydrophobic surface treatment solution, followed by an overnight incubation at 65°C. In addition, the device was disinfected by rinsing the channels three times with 75% ethanol, followed by rinsing with DI water. We equipped the device with male mini Luer fluid connectors (CS-10000095, Darwin Microfluidics) to seamlessly connect the tubing to the chip. The experiment involved the use of 1 mL syringes, filled with either oil or aqueous phase, attached to Syringe Pumps (NE-300, InfusionONE). The inlets and outlets of the device were connected to the male mini Luer fluid connectors using platinum-cured silicone tubing (SHE-TUB-SIL-11, Darwin Microfluidics), which features a 1.0 mm inner diameter and a 1.0 mm wall thickness.

This setup maintained a steady flow rate of 100 μL/h for the dispersed (aqueous) phase, split between 90 μL/h for the bacterial solution and 10 μL/h for the antibiotic solution. We prepared a bacterial

solution with a concentration of 2×10^5 CFU/mL in MH broth by adding 10% (v/v) of AlamarBlue solution. Depending on the desired ratio of dispersed to continuous (oil) phase (1:2 or 1:10), we selected a flow rate of either 200 or 1000 μL/h for the continuous (oil) phase. For the experiments, two distinct types of oil were selected for evaluation. The first choice was Fluo-Oil 7500, which was mixed with 2.5% FluoSurf Surfactant by weight. The second was Fluo-Oil 200, which was combined with 3.75% FluoSurf Surfactant by weight. We discovered that Fluo-Oil 200 required a higher concentration of surfactant to stabilize the droplets. Using a 2.5% (w/w) fluorosurfactant concentration, the droplets remained stable after generation within the microfluidic device and tubing. However, upon collection, the droplets coalesced due to disturbances encountered during transfer to the Eppendorf-type tube. A stable emulsion was achieved when the fluorosurfactant concentration was increased to 3.75% (w/w).

To conduct droplet size analysis and AST, 10 μL of droplets was dispensed onto a microscope slide and observed using a microscope (Axio Imager, Zeiss) following a 3-h incubation period at 37°C. Both bright-field and fluorescence images (EX: 510–560/EM: LP 580) were captured for the subsequent analysis. The consistency of droplet generation was evaluated by calculating the coefficient of variation (%CV) for the droplet diameters (%CV = [standard deviation/average] × 100). To minimize fluorescence bleaching, the microscope's light intensity was kept at 10%. An exposure time of 900 ms was required under a 5× lens, while a shorter exposure of approximately 500 ms sufficed for the 10× lens. All droplet detection procedures were carried out in a dark room to ensure optimal imaging conditions.

ACKNOWLEDGMENTS

The authors have nothing to report.

CONFLICT OF INTEREST STATEMENT

The authors declare no conflicts of interest.

ORCID

Xianfeng Chen https://orcid.org/0000-0002-3189-2756

REFERENCES

1. Velve-Casquillas G, Le Berre M, Piel M, Tran PT. Microfluidic tools for cell biological research. *Nano Today*. 2010;5:28-47.
2. Ng JMK, Gitlin I, Stroock AD, Whitesides GM. Components for integrated poly(dimethylsiloxane) microfluidic systems. *Electrophoresis*. 2002;23:3461-3473.
3. Qin D, Xia Y, Whitesides GM. Soft lithography for micro- and nanoscale patterning. *Nat Protoc*. 2010;5:491-502.
4. Balakrishnan HK, Badar F, Doeven EH, et al. 3D printing: an alternative microfabrication approach with unprecedented opportunities in design. *Anal Chem*. 2020;93:350-366.
5. Chen C, Mehl BT, Munshi AS, Townsend AD, Spence DM, Martin RS. 3D-printed microfluidic devices: fabrication, advantages and limitations—a mini review. *Anal Methods*. 2016;8:6005-6012.
6. Waheed S, Cabot JM, Macdonald NP, et al. 3D printed microfluidic devices: enablers and barriers. *Lab Chip*. 2016;16:1993-2013.
7. Mehta V, Rath SN. 3D printed microfluidic devices: a review focused on four fundamental manufacturing approaches and implications on the field of healthcare. *Bio-Des Manuf*. 2021;4:311-343.
8. de Almeida Monteiro Melo Ferraz M, Henning HHW, da Costa PF, et al. Potential health and environmental risks of three-dimensional engineered polymers. *Environ Sci Technol Lett*. 2018;5:80-85.
9. Oskui SM, Diamante G, Liao C, et al. Assessing and reducing the toxicity of 3D-printed parts. *Environ Sci Technol Lett*. 2016;3:1-6.
10. Carve M, Wlodkowic D. 3D-printed chips: compatibility of additive manufacturing photopolymeric substrata with biological applications. *Micromachines*. 2018;9:91.
11. Venzac B, Deng S, Mahmoud Z, et al. PDMS curing inhibition on 3D-printed molds: why? Also, how to avoid it? *Anal Chem*. 2021;93:7180-7187.
12. Comina G, Suska A, Filippini D. PDMS lab-on-a-chip fabrication using 3D printed templates. *Lab Chip*. 2014;14:424-430.
13. Chan HN, Chen Y, Shu Y, Chen Y, Tian Q, Wu H. Direct, one-step molding of 3D-printed structures for convenient fabrication of truly 3D PDMS microfluidic chips. *Microfluid Nanofluid*. 2015;19:9-18.
14. Olanrewaju A, Robillard A, Dagher M, Juncker D. Autonomous microfluidic capillaric circuits replicated from 3D-printed molds. *Lab Chip*. 2016;16:3804-3814.
15. Fritschen A, Bell AK, Konigstein I, Stuhn L, Stark RW, Blaeser A. Investigation and comparison of resin materials in transparent DLP-printing for application in cell culture and organs-on-a-chip. *Biomater Sci*. 2022;10:1981-1994.
16. Urrios A, Parra-Cabrera C, Bhattacharjee N, et al. 3D-printing of transparent bio-microfluidic devices in PEG-DA. *Lab Chip*. 2016;16:2287-2294.
17. Xu Y, Qi F, Mao H, et al. In-situ transfer vat photopolymerization for transparent microfluidic device fabrication. *Nat Commun*. 2022;13:918.
18. Ng WL, Lee JM, Zhou M, et al. Vat polymerization-based bioprinting—process, materials, applications and regulatory challenges. *Biofabrication*. 2020;12:022001.
19. Gibson I, Rosen D, Stucker B, et al. *Additive Manufacturing Technologies*. Vol 17. Springer; 2021.
20. Shrestha J, Ghadiri M, Shanmugavel M, et al. A rapidly prototyped lung-on-a-chip model using 3D-printed molds. *Organs-on-a-Chip*. 2019;1:100001.
21. O'Grady BJ, Geuy MD, Kim H, et al. Rapid prototyping of cell culture microdevices using parylene-coated 3D prints. *Lab Chip*. 2021;21:4814-4822.
22. Gong H, Beauchamp M, Perry S, Woolley AT, Nordin GP. Optical approach to resin formulation for 3D printed microfluidics. *RSC Adv*. 2015;5:106621-106632.
23. Boaks M, Roper C, Viglione M, et al. Biocompatible high-resolution 3D-printed microfluidic devices: integrated cell chemotaxis demonstration. *Micromachines*. 2023;14:1589.

SUPPORTING INFORMATION

Additional supporting information can be found online in the Supporting Information section at the end of this article.

How to cite this article: Ye M, Xue Y, Zhao H, et al. Programmable optical window bonding enabled 3D printing of high-resolution transparent microfluidic devices for biomedical applications. *Droplet*. 2025;e153. https://doi.org/10.1002/dro2.153